

Computer-controlled dynamic mode multidirectional UV lithography for 3D microfabrication

This article has been downloaded from IOPscience. Please scroll down to see the full text article.

2011 J. Micromech. Microeng. 21 035003

(<http://iopscience.iop.org/0960-1317/21/3/035003>)

View [the table of contents for this issue](#), or go to the [journal homepage](#) for more

Download details:

IP Address: 130.207.154.215

The article was downloaded on 01/02/2011 at 17:52

Please note that [terms and conditions apply](#).

Computer-controlled dynamic mode multidirectional UV lithography for 3D microfabrication

Jungkwun Kim^{1,2}, Mark G Allen³ and Yong-Kyu Yoon^{1,2,4}

¹ University of Florida, Gainesville, FL, USA

² University at Buffalo, The State University of New York, Buffalo, NY, USA

³ Georgia Institute of Technology, Atlanta, GA, USA

E-mail: ykyoon@ece.ufl.edu

Received 26 October 2010, in final form 5 January 2011

Published 1 February 2011

Online at stacks.iop.org/JMM/21/035003

Abstract

Computer-controlled dynamic mode multidirectional ultraviolet (UV) lithography has been demonstrated using a collimated UV light source, a substrate-holding stage equipped with two stepper motors (one for tilting and the other for rotation), a controller with programming software and a laptop computer. The tilting and rotational angles of the stage in motion are accurately controlled during UV exposure as programmed by the user to produce complex three-dimensional (3D) microstructures. Process parameters include the initial and final tilting and rotational angles of the stage, and the relative angular velocities of the two motors in addition to the normal fabrication process parameters of UV lithography such as optical dose, baking time, and developing time and condition. Symmetric patterns can be generated by a simple synchronous mode dynamic operation, where both the angular velocities of the tilting motion and the rotating motion are set equal or harmonically related. More complex and non-symmetric patterns can be obtained using a piecewise synchronous mode, where the relationship between the angular velocities of the two motors is described not with a single coefficient but with a set of coefficients. 3D structures fabricated from the synchronous mode operation include the four-leaf clover horn and the cardiac horn while the ones from the piecewise synchronous mode are a vertical triangular slab, a screwed wind vane and arbitrary shape horns. Ray trace simulation has been performed using a mathematical tool in a spherical coordinate system and the simulated 3D patterns show good agreement with the fabricated ones.

(Some figures in this article are in colour only in the electronic version)

1. Introduction

Ultraviolet (UV) lithography is one of the most commonly used methods for microfabrication. Equipment utilized in UV lithography is relatively inexpensive compared to that of the x-ray lithography or laser process and can produce a large volume of microstructures with a photosensitive polymer [1–4]. Various three dimensional (3D) fabrication processes using UV lithography were introduced in the early 1990s [5–8], where mostly positive photoresists were utilized for patterning micromolds and they are filled with metals by electroplating.

Those processes show relatively thick structures but the patternable polymer thickness of a single-step coating is limited to approximately 50 μm or less due to the relatively large optical absorption of the positive photoresist.

Since a photopatternable negative-tone epoxy resin, SU-8, was introduced in the mid-1990s, it has been very widely used to fabricate 3D microstructures with a height of hundreds of micrometers and an aspect ratio of greater than 10 using UV or near-UV light sources [9–12]. By a single spin coating, SU-8 can be formed as thick as 600 μm and as thin as 500 nm [13]. Also SU-8 thicker than 600 μm has been demonstrated using the process of weighing and self-planarization on a leveled

⁴ Author to whom any correspondence should be addressed.

hotplate [14]. Applications using thick SU-8 structures include microfluidic channels, passive radio frequency components, integrable antennas, etc [15–20].

In 1994, an inclined UV lithography scheme with a positive photoresist was reported for the fabrication of a microturbine blade [21]. The fabricated structure showed a relatively small inclined angle of approximately 10° and a structure height of up to $120\ \mu\text{m}$ with the limitation of the relatively high refractive index and high absorption rate of the positive photoresist used. Recently, inclined UV lithography has been applied to SU-8, producing many unusual complex structures such as a vertical screen filter, a mixer and a cell sorter by multiple groups with a maximum inclined angle of 36° in air environment [22–24] and greater than 36° in the environment of a different refractive index material such as water, heptanes and glycerol [25–27]. Very recently, multidirectional UV lithography with a semi-manual moving stage has been demonstrated with SU-8 to produce more complex 3D structures [28–34] with merits of fabrication simplicity, cost effectiveness and manufacturability. However, the earlier demonstration for inclined and multidirectional UV lithography has been performed in either a pure static mode, in which the tilted stage is fixed during each UV exposure, or a partial dynamic mode, in which the tilted angle is fixed while the stage keeps rotating at a constant speed producing only axisymmetric structures.

In this work, the multidirectional UV lithography process has been further explored in a fully computer-controlled dynamic mode scheme, where the substrate-holding stage under an UV light source is independently controlled for tilting and rotating by attached motors as programmed by the user during UV exposure. While the previous inclined/multidirectional UV lithography [28, 29] has demonstrated limited motion of the UV exposure stage so that the projectable 3D microstructures are relatively simple, such as inclined pillars or horn structures, the dynamic mode multidirectional UV lithography scheme here has demonstrated more complex structures with additional process parameters such as continuously variable tilting and rotational angles and their angular velocities. Unusual 3D microstructures with non-axisymmetric curved sidewalls such as a cardiac-shaped horn, screwed wind vanes with double and quadruple blades, and arbitrarily shaped horns are demonstrated. Ray-tracing simulation with analytical equations has been performed and the simulated 3D structures are compared with experimental results.

2. Computer-controlled dynamic mode multidirectional UV lithography

2.1. Operational concept

Figure 1 shows a schematic of dynamic mode multidirectional UV lithography. A glass substrate with a pre-patterned chromium layer and a photoresist layer on the chromium side is placed under UV exposure. Note that the substrate is turned over and mounted on the dynamic stage with tilting and rotation functionality. Since the glass substrate with the

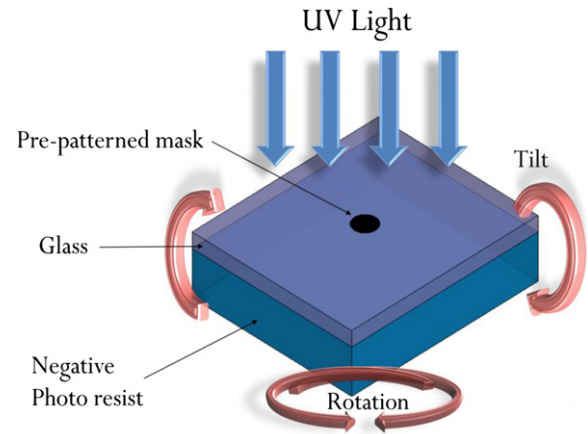


Figure 1. Dynamic mode multidirectional UV exposure.

pre-patterned chromium layer also serves as a self-aligned photomask (this is called a reverse or backside exposure scheme since the light comes through the substrate) [30], a good contact without a gap between the substrate and the photoresist layer is secured. The dynamic mode operation involves the discrete or continuous movement of the stage during UV exposure. The tilting angle can be varied between -90° and $+90^\circ$ with the horizontal plane as a reference plane while the rotational angle can change continuously or discretely clockwise or counterclockwise unlimitedly. The combination of the tilting angle and the rotational angle of the stage renders the ray trace of the incident light in the photoresist slab through a clear pattern of the photomask. The tilting and rotational movement in this work is realized by computer-controlled motors attached to the tilting and rotational axes as shown in figure 2. The system of the dynamic mode multidirectional UV lithography process is composed of the collimated UV light source, the movable stage with two motors for tilting and rotation, a controller with software and a laptop computer for programming. After programming the software for a desired stage movement, the main computer sends a command to the controller which is connected between the computer and two stepper motors. The controller operates the two stepper motors which are attached to the stage for tilting and rotational angle control.

2.2. Spherical coordinate system for ray tracing

When UV light is incident on the sample substrate with an incident angle of θ_i , it is refracted first at the interface between air and the glass substrate and second at the interface between the glass substrate and the photoresist because of the difference of refractive indices of air, glass and photoresist. A ray tracing of the refracted light is schematically drawn as shown in figure 3. The relationship between the incident angle and the final refracted angle is described using Snell's law and the final refracted angle is expressed using the incident angle and the refractive indices of air and the photoresist. Because of the high refractive index (1.67) of SU-8 compared to that of air, the maximum achievable refracted angle in this system is calculated as no more than 36° [30]. The maximum

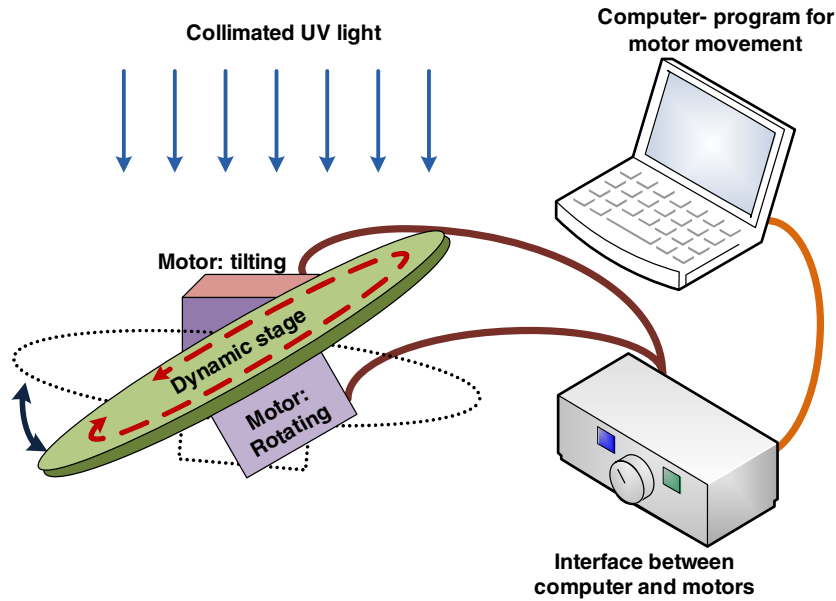


Figure 2. Schematic of the dynamic mode multidirectional UV lithography system.

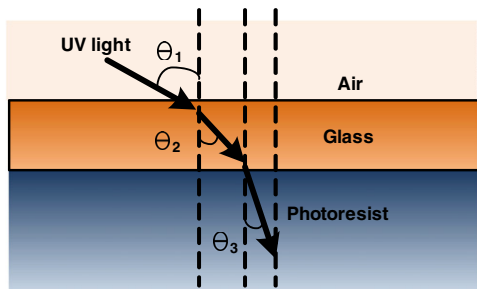


Figure 3. Schematic of ray tracing at the interfaces of the materials with different refractive indices.

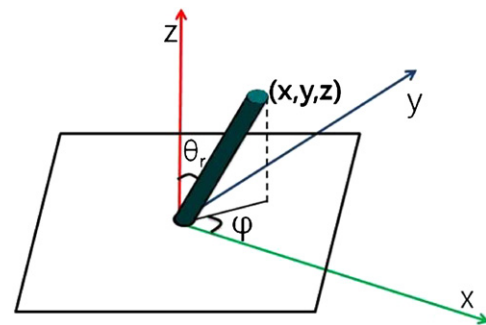


Figure 4. Spherical coordinate system used to describe ray trace in the analytical form.

refracted angle determines the maximum patternable tilting angle of a 3D structure. To mathematically describe the refracted UV light path, a spherical coordinate system is adopted as shown in figure 4. The ray trace of the refracted light through a circular transparent window in a dark field photomask has a refracted angle (or a latitudinal angle) θ_r from the vertical axis and a longitudinal angle φ from the x axis in the x - y plane. Therefore, the x , y and z values of the trace in the Cartesian coordinate system (x , y , z) can be described by equations (1)–(3) [30]:

$$x = z \tan(\theta_r) \cos(\varphi) \tag{1}$$

$$y = z \tan(\theta_r) \sin(\varphi) \tag{2}$$

$$z = z \tag{3}$$

$$x^2 + y^2 = (z \tan(\theta_r))^2, \tag{4}$$

where θ_r is the refracted angle (tilting or latitudinal angle) and φ the rotational angle (or longitudinal angle).

Equation (4) derived from the sum of the square of equation (1) and the square of equation (2) describes the relationship between x and y in the x - y plane for a given

structure height z . Geometrically, equation (4) represents a circle with a radius of $z \tan(\theta_r)$. If the tilting angle θ_r is constant, e.g. θ_{r0} during the process, the locus in the x - y plane at thickness z_1 will be a circle with a radius of $z_1 \tan(\theta_{r0})$. In 3D, a horn with a circular locus in the x - y plane will be formed. When θ_r is varying, the generated locus in the x - y plane will be different from a circle but show various patterns determined as a function of the angular velocities of tilting and rotational angles, and time, and therefore generating various 3D horn structures.

Since the latitudinal angle (θ_r) and the longitudinal angle (φ) can be changed in dynamic mode multidirectional lithography, θ_r and φ can be expressed as a function of time (t) and angular frequency (ω) as variables. By selecting different θ_r and φ movement, there is an unlimited number of traces available, which can also be described in mathematical forms. For example, if the latitudinal angle θ_r changes with the initial value θ_{r0} and angular velocity ω_1 , and the longitudinal angle φ changes with the initial value φ_0 and angular velocity ω_2 , θ_r and φ are described by equations (5) and (6), respectively:

$$\theta_r(\omega, t) = \theta_{r0} + \omega_1 t \tag{5}$$

$$\varphi(\omega, t) = \varphi_0 + \omega_2 t, \tag{6}$$

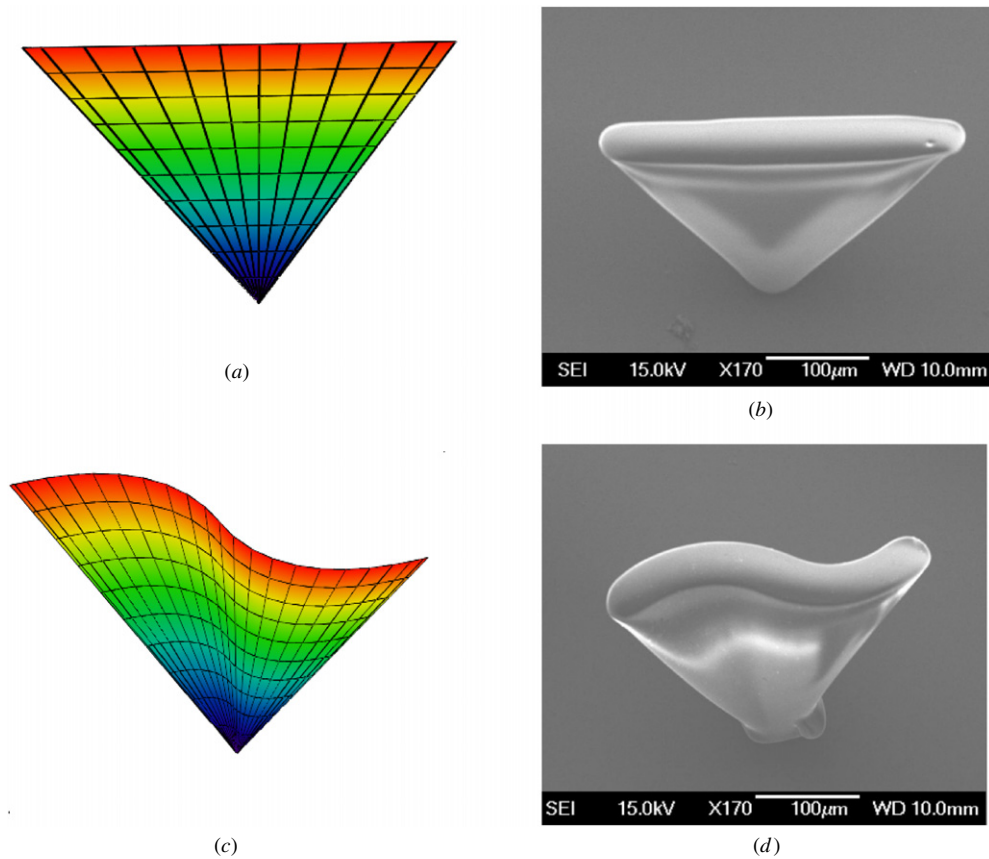


Figure 5. MathCAD simulation and fabrication result. (a) Simulation result of the triangular slab. (b) SEM image of the fabricated triangular slab. (c) Simulation result of the screwed wind vane with double blade. (d) SEM image of the fabricated screwed wind vane with double blades.

where θ_{r0} is the initial tilting angle, φ_0 the initial rotational angle, ω_1 and ω_2 the angular velocity of the tilting and rotational angle of the stage, respectively, and t the operation time.

2.3. Ray tracing

3D ray tracing is performed using equations (1)–(6) with mathematical software MathCAD (Parametric Technology Corporation, version 14). Some photolithography simulations include diffraction, reflection and absorption effects to predict the surface profile of the fabricated SU-8 structures [36, 37]. Such optical effects in modeling have not been included in this work. Rather, the focus is placed on the automation of the multidirectional UV lithography system and the demonstration of overall ray trace for feasible 3D microstructures with new variables such as initial and final angles, angular velocity, synchronization, etc. The demonstrated MathCAD projection is an adequate approach in dynamic mode multidirectional UV lithography for the prediction of overall 3D microstructures under a continuously varying tilting and rotational environment. As an example of simulation, a vertically standing triangular slab is shown in figure 5(a). In the case of a triangular slab, the rotational angle is fixed ($\omega_2 = 0$) while the tilting angle is varied. The tilting angle ($\theta_r = \theta_{r0} + \omega_1 t$) is set to vary from -30° to 30° .

The simulated result in figure 5(a) has a flare angle of 60° and the triangular slab is parallel to the y axis with a rotational angle ($\omega_2 t$) of zero. Figure 5(b) shows a fabricated triangular slab. $300 \mu\text{m}$ thick SU-8 is applied on a patterned glass substrate. After 3 h soft baking and 1 h cooling down to room temperature, dynamic mode multidirectional UV lithography is applied with a continuous tilting angle of the substrate-holding stage from -56° to 56° and no rotational movement. The tilting angle of the stage (56°) has been determined considering the refractive index of SU-8 of 1.67 to achieve a tilting angle of the structure (30°) using Snell's law. The fabricated triangular slab in figure 5(b) shows good agreement with the simulated result in figure 5(a).

Also a screwed wind vane in figures 5(c) and (d) has been demonstrated as an example to show the combination of variable tilting and rotational angle. The tilting and rotational angles change between -30° and 30° and between -45° and 45° , respectively, in a synchronous fashion. In this case, the angular velocity of the rotational angle is 1.5 times faster than that of the tilting angle since the tilting angle variation is 60° (-30° – 30°) while the rotational angle variation is 90° (-45° – 45°). The relationship between the rotational angular velocity and the tilting angular velocity is expressed as follows:

$$k = \omega_2 / \omega_1. \quad (7)$$

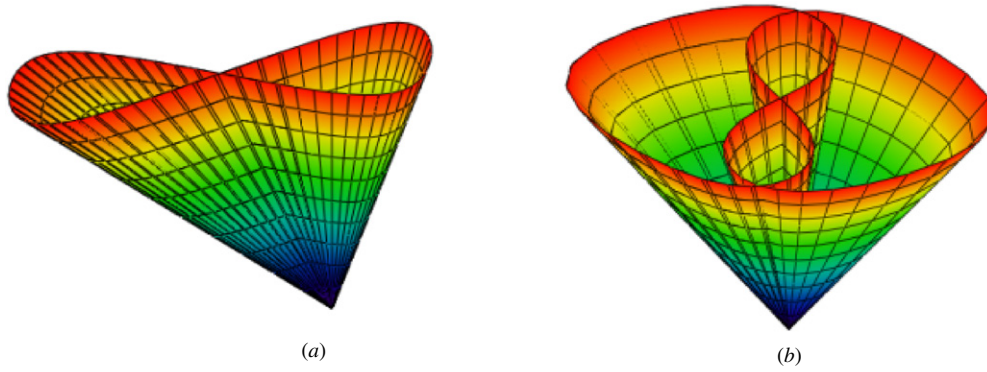


Figure 6. Different constant k produces different geometry with same tilting and rotational angles. $-30^\circ < \theta_r < 30^\circ$: (a) bowtie horn ($k = 1$); (b) horn with the embedded figure 8 ($k = 2$).

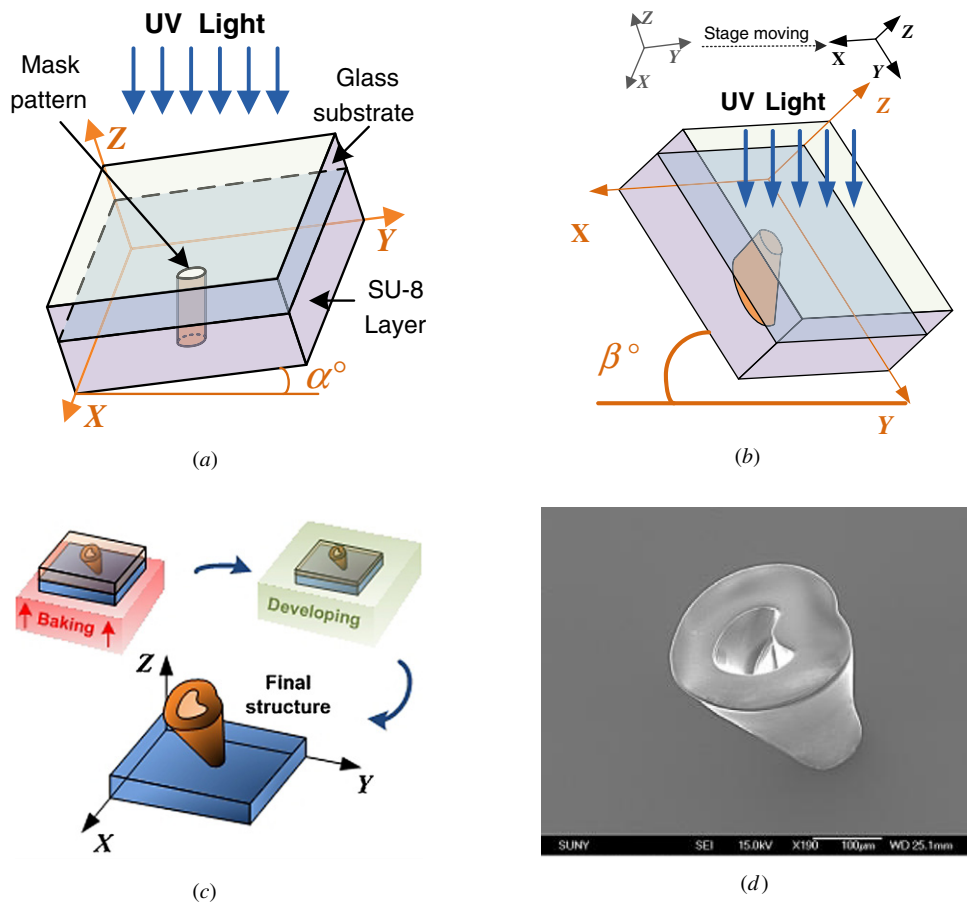


Figure 7. Fabrication process. (a) Expose the sample with an initial tilting angle of α° and a continuous rotational angle of 180° . (b) Change the tilting angle during continuous rotation. (c) Post-exposure bake at 95°C to crosslink SU-8 for an hour and develop it in developer. (d) Reveal the asymmetric cardiac horn structure.

The velocity constant, k , will be one of the 3D design variables for synchronous operation. With a given range of the tilting and the rotational angles, different k can produce different 3D geometries. For example, when the tilting angle is set from -30° to 30° and the rotational angle from 0° to 360° , two different velocity constants such as 1 and 2 produce different structures. ‘Bowtie horn’ and ‘horn with embedded figure 8’ structures have been produced with a velocity constant (k) of 1 and 2 as shown in figures 6(a) and (b), respectively.

3. Fabrication process

3.1. General fabrication description

The dynamic mode multidirectional UV lithography process with SU-8 follows the same procedure as the conventional UV lithography process such as photoresist coating, soft baking, UV exposure, post-exposure baking and developing. The major difference between dynamic mode multidirectional UV lithography and conventional lithography lies in the UV exposure step. The dynamic mode process has the sample

holding stage dynamically moving during UV exposure while the conventional one has the stage remaining static. Depending on its dynamic motion, various 3D ray trace patterns can be formed from the dynamic mode process. As an example of the dynamic mode multidirectional UV lithography process, the fabrication of a cardiac horn structure using SU-8 has been demonstrated as shown in figure 7. A chromium-coated glass plate is used as a substrate as well as a photomask for backside exposure. After patterning the chromium photomask layer, SU-8 is coated on the chromium side of the substrate to a thickness which will ultimately define the height of the structure. A 300 μm thick SU-8 layer shown in figure 7 is applied using the dispensing and self-planarization process consisting of precisely dispensing SU-8 on the substrates with the density of SU-8, the applied area, and the weight of the applied SU-8 known to control the thickness. During soft baking, the substrate is placed on a well-leveled hotplate surface. After the SU-8-coated sample is baked at 95 °C for 3 h and cooled down to room temperature, the substrate is turned over and exposed at different angles where the tilting and rotational angles dynamically change as programmed by the user, as shown in figures 7(a) and (b). An optical dose of 12 000 mJ cm^{-2} has been applied on the sample. Exposure is followed by a post-exposure bake step at 95 °C to crosslink SU-8 for an hour and natural cooling of the sample is performed at room temperature for an hour. A development step then reveals complete projected structures as shown in figure 7(c). A fabricated sample structure is shown in figure 7(d).

3.2. System apparatus

The overall system apparatus consists of a collimated UV light source (LS 30, OAI Inc.), a dynamic stage with two degrees of freedom for tilting and rotation and a stage controller with a computer as shown in figure 8(a). The light source produces intense, uniform, collimated UV with a wavelength of 365 nm. The exposing power from the UV light source is set as 20 mW cm^{-2} with a uniform beam over a circular area of 4 inch diameter. The dynamic stage as shown in figure 8(b) is designed for two operating motions: stage tilting and rotation. The designed movable stage under UV light has a larger area than the beam size (4") of the UV light source and a circular aluminum plate with 5.5" diameter has been chosen as a substrate holder for light weight purpose to minimize load to the motor. The circular aluminum plate is attached to the axle of a stepper motor, which enables the rotational motion of the plate. For tilting motion, a U-shape metal frame is prepared and the top open portion is bridged with a shaft which is directly connected to the axle of another motor. Finally, the circular aluminum plate with the first motor is mounted on the shaft as shown in figure 8(b). Two motors are connected to a controller box with extended cables. The rotational motor allows full 360° rotation both clockwise and counterclockwise. The tilting motor allows the stage to tilt to -90° and 90° with regard to the horizontal plane. Two stepper motors (MD-2A, Arrick Robotics Inc.) have been chosen. The size and the weight of the motor are 2.24" \times 2.24" \times 2" and 21 ounces, respectively. The step

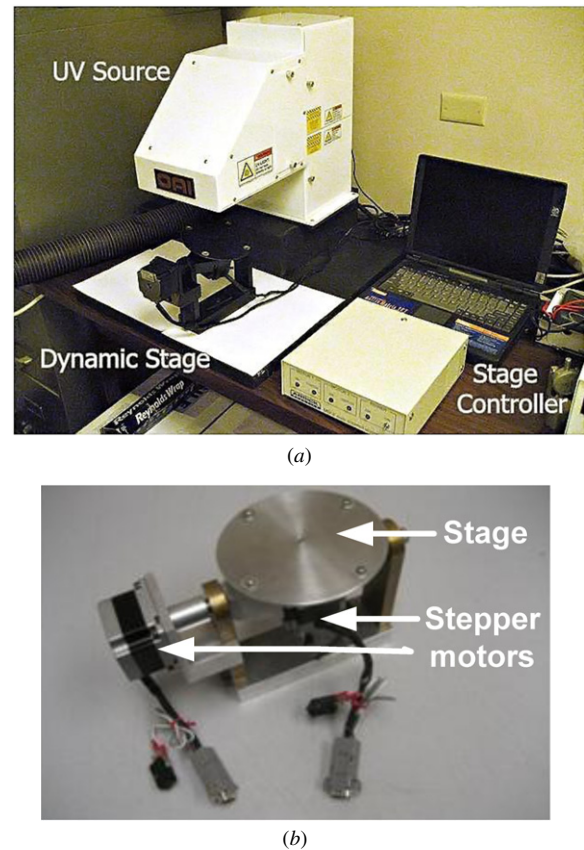


Figure 8. System setup. (a) System apparatus. (b) Dynamic stage.

size of the motor is designed as 0.9 degree for half a step and 1.8 degree for a full step with 5% accuracy. Also the stepper motors have sufficient power (50 oz in^{-1} for both pull-in and pull-out torque) to rotate and tilt the entire stage with a sample. The motor-holding frame is made of iron, which gives weight to firmly hold the stage during the dynamic movement. Also the computer program allows the operator to control the dual stepper motor system as preprogrammed or interactively. The control parameters are motor speed (5–20 rpm), direction (clockwise or counterclockwise) and the initial and ending angles.

4. Modes

One of the advantages of the dynamic mode multidirectional UV lithography process is that the stage is dynamically moving during exposure by the attached motors and computer and therefore complex 3D ray trace patterns can be formed in the polymer slab. Depending on the initial and final angular positions and the tilting and rotating velocities of the dynamic stage, an infinite number of 3D ray traces can be produced with the same photomask pattern. The multidirectional UV lithography process is categorized as three different modes depending on the motion of the stage: a static mode, a synchronous mode and a piecewise synchronous mode. In the static mode, the stage does not move during exposure but poses in a certain tilting and rotating angle. The products of the static mode process include vertical or inclined 3D pillars

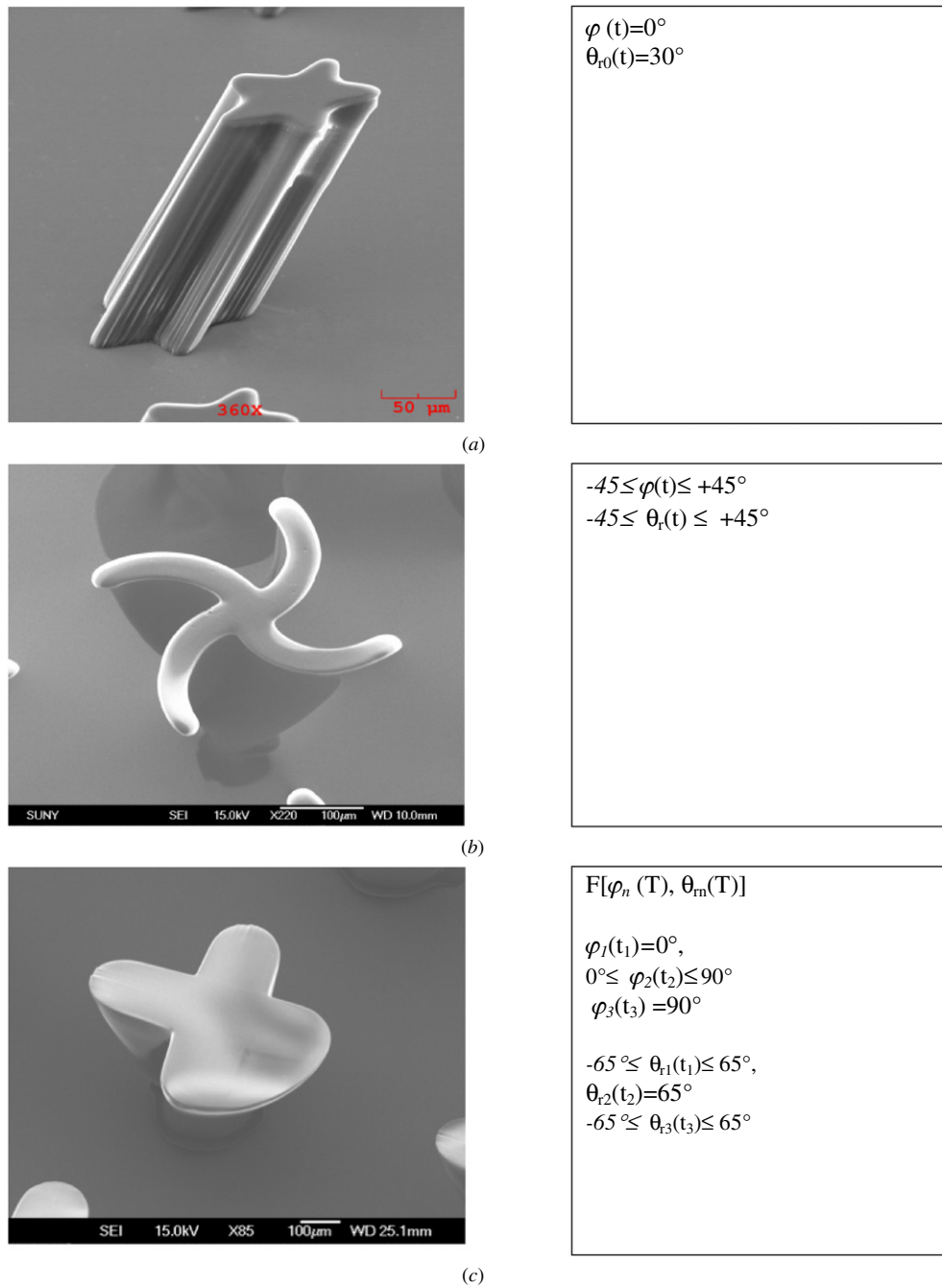


Figure 9. Different operation modes of multidirectional UV lithography: (a) static mode, (b) synchronous mode, (c) piecewise synchronous mode.

with various photomask patterns [30]. Figure 9(a) shows a star-shaped inclined micropillar as an example. UV light is exposed to the substrate with an inclined angle of 58° from the sample plane and a final inclined angle of 30° .

The synchronous mode operation can be obtained when the angular velocities of two motors for tilting and rotating movements are in a harmonic relationship. The ratio between the rotational and tilting angular velocities has been defined as a constant k in equation (7), where k is a rational number. A triangular slab can be formed using the periodic tilting motion with an angular velocity of ω_1 and no rotational movement, i.e. $\omega_2 = 0$, where $k (= \omega_2/\omega_1)$ is zero. A wind vane structure

can be obtained by the same ω_1 and ω_2 ($k = 1$) with the same tilting and rotational angular span, or different ω_1 and ω_2 and different tilting and rotational angular spans. Figure 9(b) shows a microscale double-bladed screwed wind vane as an example of the synchronous mode operation. The thickness of SU-8 is $250 \mu\text{m}$ and the mask pattern is a circle with a diameter of $40 \mu\text{m}$. The synchronous operation has both tilting and rotating angles varying from -45° to 45° with an angular velocity of 10 rpm for both motors ($k = 1$) until a sufficient optical dose is provided. The fabricated structure as shown in figure 9(b) has a flare angle of 50° with curved sidewalls. Some structures fabricated using the synchronous operation

are symmetric with respect to the vertical axis (z axis). Some x - y plane patterns show traces similar to Lissajous figures in an oscilloscope for different phase angles and angular velocities of tilting and rotating motors.

3D microstructures with non-symmetric shapes in an x - y plane can be fabricated using piecewise synchronous operation, where multiple sections of synchronous operation are performed in sequence to construct non-symmetric structures. These sequential operations are performed using the attached microcontroller and computer. Figure 9(c) shows a horn with a rabbit face as a relatively simple example for the piecewise synchronous mode operation. The 3D structure has been implemented using three sections of synchronous operation: an operation for a vertical triangular slab as shown in figure 5(b), one for a quarter segment of a circular horn, and one for another vertical triangular slab formation with a phase offset of 90° in rotational angle from the first triangular slab. The first sequence starts with the fabrication of a vertical triangular slab, where the stage tilts between -65° and 65° with zero rotational angle. The second sequence has the variation of the rotational angle from 0° to -45° (counterclockwise rotation) with a fixed tilting angle of 65° . The third sequence starts from the ending point of the second sequence with tilting angle variation from 65° to -65° and a fixed rotational angle. Three synchronous operations are sequentially repeated back and forth until a sufficient optical dose is applied to the sample. Subsequent post-exposure bake and development realize the 3D microstructure.

4.1. Algorithm for a synchronous mode operation

In the synchronous mode operation, the angular velocities of two stepper motors are harmonically related and periodically repeated as programmed. For programming the desired sequential motion of the motors, an operation algorithm is prepared. For example, an algorithm sequence for screwed wind vane fabrication is described as shown in figure 10. The algorithm flowchart starts from the variables' definition such as a tilting angle of 0° and a rotational angle of 0° . Then the tilting and rotational angles are increased until the tilting and rotational angles reach 30° and 45° , respectively, which are monitored in the conditional block. The next command block starts to decrease the maximally reached tilting and rotational angles to the position of the original point where UV exposure for the half portion of the screwed wind vane is completed. The other part of the flowchart shows the command and the condition for the other half portion of the screwed wind vane in a different direction. The process is repeated back and forth continuously and the UV exposure dose can be controlled by the timer and the shutter of the system.

4.2. Algorithm for a piecewise synchronous mode operation

Horn type 3D structures with non-symmetric and arbitrary patterns can be implemented using the piecewise synchronous mode operation, where an appropriate segmentation is necessary. For example, figure 11 shows segmentation for a horn structure with characters of 'UB' for which a total of 19 segmentations has been used. Each segment operated in

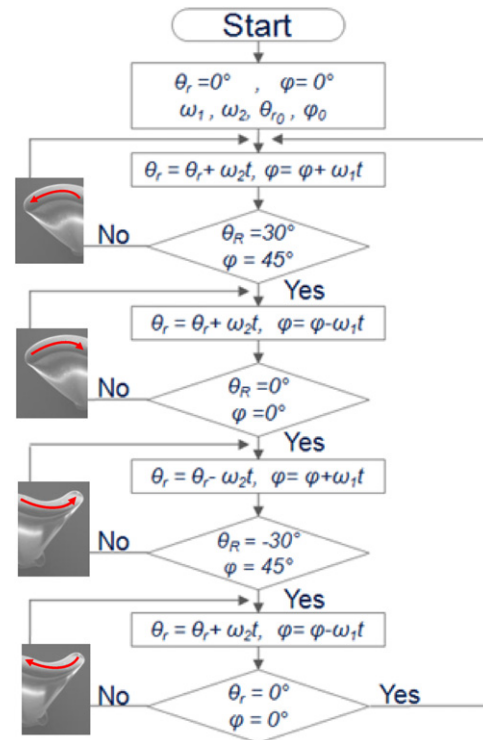


Figure 10. Algorithm for the fabrication of a screwed wind vane.

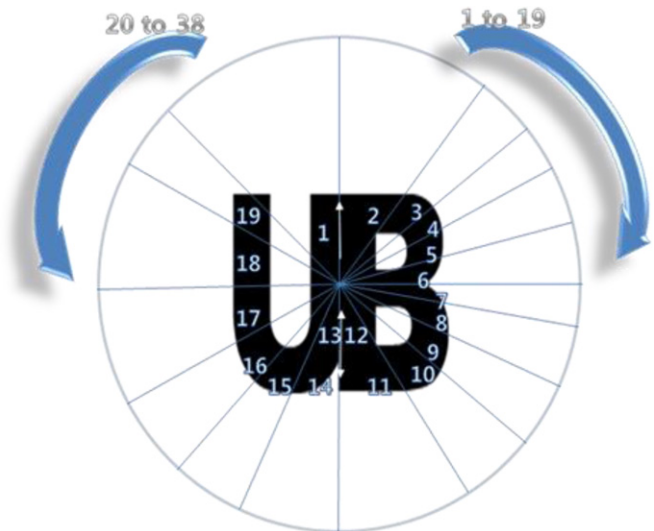


Figure 11. Segmentation of the characters 'UB'.

a synchronous mode is analyzed, calculated and programmed for its tilting and rotational angle variation with each velocity constant k . The center point of the 'UB' is set as the origin (tilting angle = 0°). Considering the refractive index of 1.67 and the maximum achievable inclined angle of approximately 37° for SU-8 [30], the longest distance from the center point for the characters is safely designed within the process limit. The rest of the tilting angles of each segment are determined between 0° and 37° depending on its distance from the center point. For the rotational angles of 'UB' characters, the y -axis line from the center point is set at 0° as reference.

Table 1. ‘UB’ lettering algorithm chart.

Segment no.	Tilting			Rotation		
	Incident (deg)	Refracted (deg)	Program	Designed (deg)	Resultant (deg)	Program
1	65.85	33.12	36.80	0	0	0
2	14.15	8.42	9.36	36	−36	−40.00
3	5.62	3.36	3.73	15	−15	−16.67
4	0	0.00	0.00	9	−9	−10.00
5	−17.05	−10.11	−11.24	13.5	−13.5	−15.00
6	−35.68	−20.44	−22.72	14.5	−14.5	−16.11
7	42.74	23.98	26.65	10	−10	−11.11
:	:	:	:	:	:	:
:	:	:	:	:	:	:
:	:	:	:	:	:	:
35	0	0.00	0.00	−9	9	10.00
36	−5.62	−3.36	−3.73	−15	15	16.67
37	−14.15	−8.42	−9.36	−36	36	40.00
38	−65.85	−33.12	−36.80	0	0	0.00

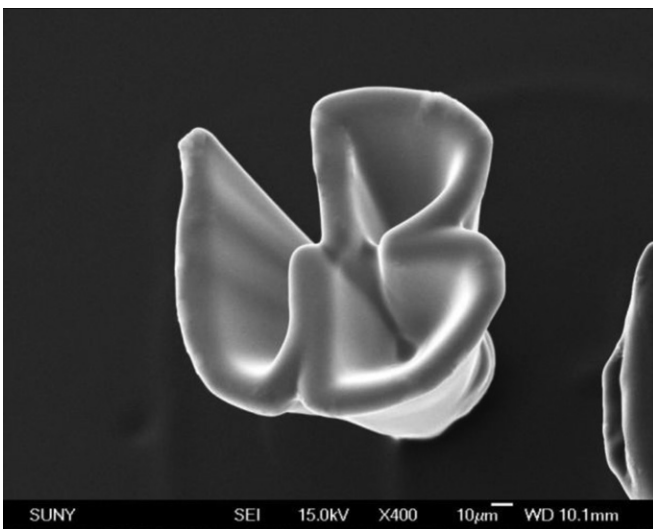


Figure 12. SEM image of the fabricated ‘UB’-shaped horn.

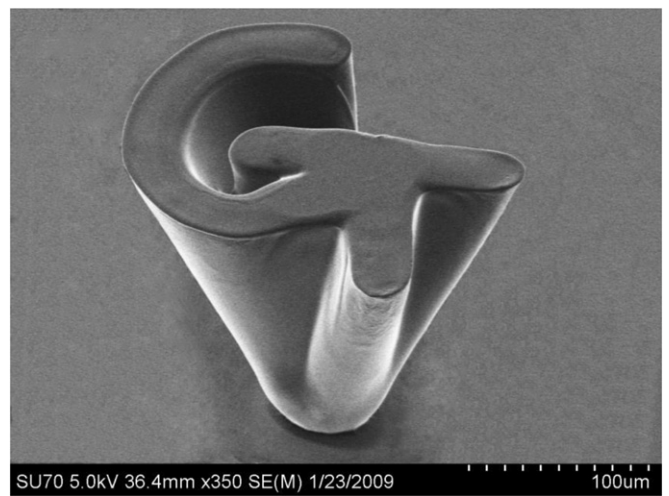


Figure 13. SEM image of the fabricated ‘GT’-shaped horn.

Each segment is assigned a rotational angle. In the case of segment no 1, for example, the tilting angle increases from 0° to 65.85° during UV exposure while the rotational angle is fixed. In segment no 2, the tilting angle changes from 65.85° to 80.0° while the rotational angle decreases from 0° to −36° (counterclockwise). In a similar manner, all 19 segmentations are conducted in sequence and the stage returns back to the origin point in the reverse order. All the designed incident angles of the UV light are converted into refracted angles using Snell’s law and are shown in the third column of table 1. Note that the measured rotational angles are related to antipodal points and the designed rotational angles need to be converted into negative values with 180° phase shift. The rotational and tilting angles required are determined and converted into the program language for the stage controller to operate two stepper motors. The rotational and tilting angles for ‘UB’ are summarized in table 1. Figure 12 shows the micro ‘UB’ from the design segmentation of figure 11. In a similar way, the micro ‘GT’ structure is successfully fabricated as well using the piecewise synchronous mode operation as shown in figure 13.

5. Results and discussion

Various 3D microstructures fabricated using automated multidirectional UV lithography are summarized in table 2 with the name of the pattern, the condition of the tilting and the rotational angles, the 3D ray trace plot by MathCAD (PTC, Inc.) and the corresponding fabricated structure. The vertical reverse triangular slab is shown in the second row with refracted tilting angle variation from −30° to +30° without rotation. Note that the tilting angle for the dynamic stage is varied up to approximately 58° to result in 30° after refraction. A quadruple reverse triangular slab in the third row is fabricated with two discrete longitudinal angles φ of 0° and 90°. A cardiac horn is demonstrated in the fourth row. With an initial tilting angle of −5°, the stage dynamically moves to a tilting angle of 75° at an angular velocity of ω_2 while rotating at a constant angular velocity of ω_1 in a synchronous mode with both ω_1 and ω_2 of 10 rpm until a desired dose is supplied to the photoresist layer.

3D structures with curved sidewalls are also demonstrated such as screwed wind vanes with double blades and quadruple blades in the fifth and sixth row, respectively. For the screwed wind vane with double blades, the angular velocity conditions

Table 2. Dynamic mode multidirectional UV lithography with a continuously varying rotational and tilting substrate.

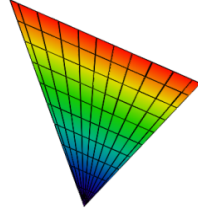
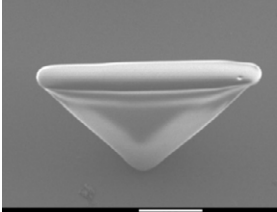
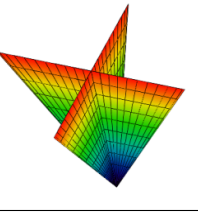
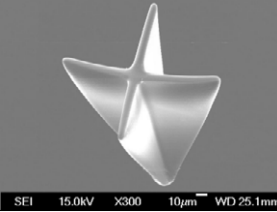
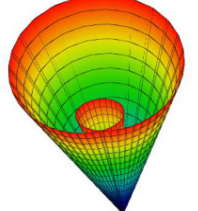
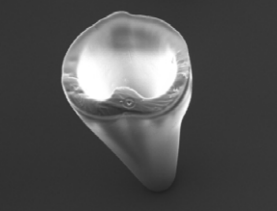
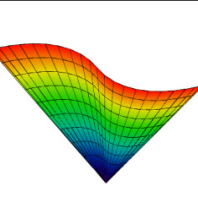
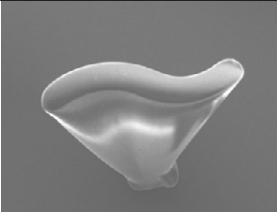
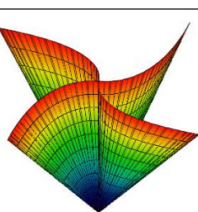
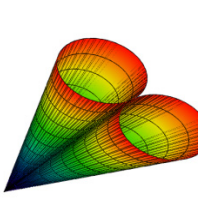
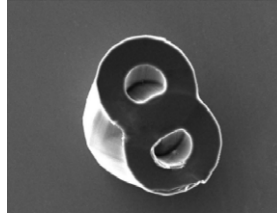
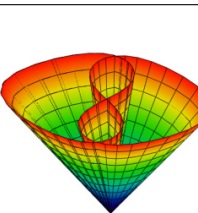
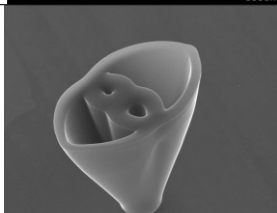
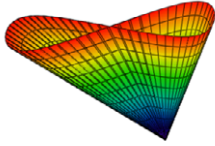
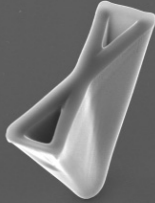
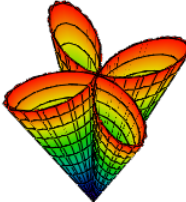
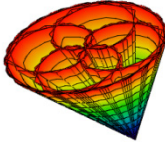
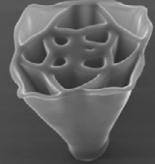
Pattern	Refracted angle	Angle	3-D Ray trace	Fabricated structure
Vertical reverse triangular slab	$-30^\circ < \theta < 30^\circ$	$\varphi = 0$		
Quadruple triangular slab	$-30^\circ < \theta < 30^\circ$	$\varphi = 0, 90^\circ$		
Cardiac horn	$-3^\circ < \theta < 30^\circ$ $\theta = \theta_{r0} \cos \omega_2 t$	$\varphi = \omega_1 t$		
Screwed wind vane with double blades	$-30^\circ < \theta < 30^\circ$ $\theta = \theta_{r0} \cos \omega_2 t$	$0 < \varphi < 45^\circ$ $\varphi = \omega_1 t$		
Screwed wind vane with quadruple blades	$-30^\circ < \theta < 30^\circ$ $\theta = \theta_{r0} \cos \omega_2 t$	$0 < \varphi < 45^\circ,$ $90^\circ < \varphi < 135^\circ$ $\varphi = \omega_1 t,$ $90^\circ + \omega_1 t$		
Figure '8' horn	$\theta = -30^\circ, 30^\circ$ $\theta = \theta_r \cos \omega_2 t$	$\varphi = \omega_1 t$		
Pattern with embedded figure '8'	$-30^\circ < \theta < 30^\circ$ $\theta = \theta_r \cos \omega_2 t$	$k=2$ $\varphi = \omega_1 t$		

Table 2. (Continued.)

<p>Bowtie horn</p>	<p>$-30^\circ < \theta < 30^\circ$ $\theta = \theta_r \cos \omega_2 t$</p>	<p>$k=1$ $\varphi = \omega_1 t$</p>		
<p>Four leaf clover horn</p>	<p>$-30^\circ < \theta < 30^\circ$ $\theta = \theta_{r0} \cos \omega_2 t$</p>	<p>$k=0.5$ $\varphi = \omega_1 t$</p>		
<p>La flor horn</p>	<p>$-30^\circ < \theta < 30^\circ$ $\theta = 30^\circ$ $\theta = \theta_{r0} \cos \omega_2 t$</p>	<p>$k=1.5, 0$ $\varphi = \omega_1 t$</p>		

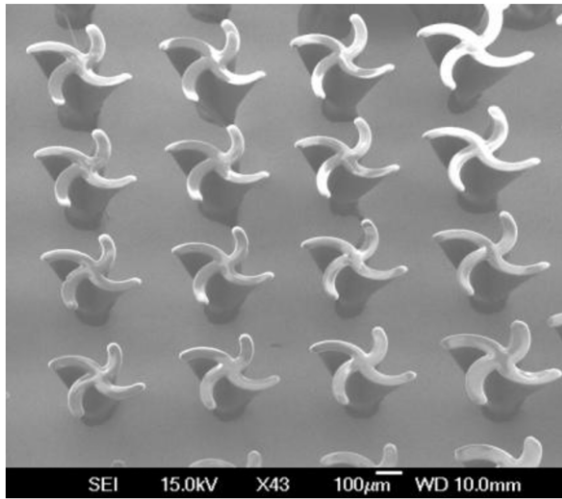
have been described in section 2.3. For the quadruple blades, the screwed wind vane process is repeated twice with a longitudinal angle offset of 90° after exposure for the first screwed wind vane. The figure ‘8’ horn structure in the seventh row is fabricated by creating two matching horns where the rotational angle is varied from 0° to 360° while the initial tilting angle of -30° is set for the first horn and the process is repeated with a latitudinal offset angle of 60° from the initial position.

The different k values of 2, 1 and 0.5 with the same angular variation range result in different 3D geometries such as a horn with embedded figure ‘8’, a bow tie horn and a four-leaf clover horn from the eighth to tenth row, respectively. The 11th row shows an artistic multilayer horn called ‘la flor horn’ meaning a flower, using two different angular velocity constants and the combination of the synchronous and piecewise synchronous mode operation. The inner four horns are fabricated with an angular velocity constant of 1.5 starting from the origin and the outer horn is fabricated using a rotational velocity of 20 rpm and a fixed tilting offset of 30° where the angular velocity constant k is infinite. The fabricated 3D structure is slightly deformed compared to the simulated plot mainly attributed to too short an UV exposure and over-development resulting in the polymer swelling effect [38], where the polymer is half-way cross-linked and is susceptible to deformation during or after the development step. Since the multi-horn structure is fabricated using the backside exposure scheme, the cross-linking quality of the SU-8 polymer at the lower portion of the structure is good and no prominent deformation is observable.

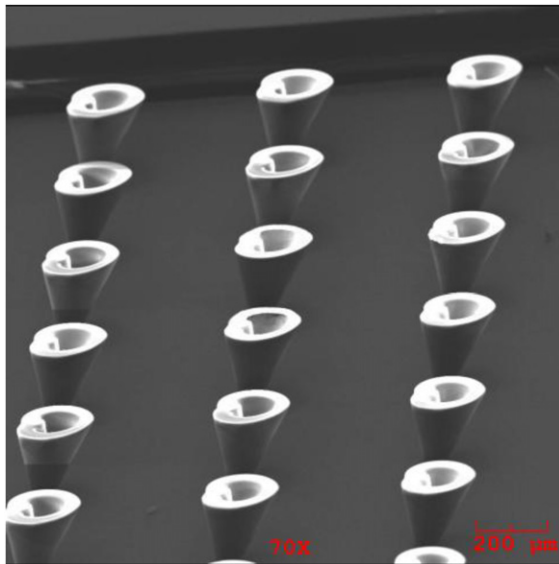
However, the UV dose at the upper portion of the structure is relatively weak and subject to the swelling effect during development, resulting in deformation during the rinse and drying step. A significant deformation is observed in the ‘la flor horn’.

Most 3D structures in table 2 are fabricated using the conventional UV lithography fabrication steps as described in the previous section. In this study, the refraction effect has been included for ray trace simulation with a refractive index of SU-8 of 1.67 and the simulated 3D shapes show good agreement with the fabricated ones. However, the diffraction effect has not been included in process modeling. The diffraction effect is large when the optical mask pattern size is smaller than or comparable with the wavelength of the light source, which is not the case in this study. For instance, the pattern size used here is $40\text{--}100\ \mu\text{m}$ and is much larger than the wavelength of i -line (365 nm) we used for the experiment. The diffraction effect is expected to be significant if the multidirectional process were to be applied to nanopatterns, which will be a good research topic for the future.

Post-expose bake (PEB) is utilized to accelerate the cross-linking of polymer. As far as the thermal energy required for cross-linking is sufficient, the excess of the thermal energy by extended PEB time or temperature does not affect much the overall shape of the microstructures. In this study, PEB has been performed at 95°C for an hour in most processes unless other specification has been indicated. The parametric analysis of PEB has not been performed. Meantime, the simple ray



(a)



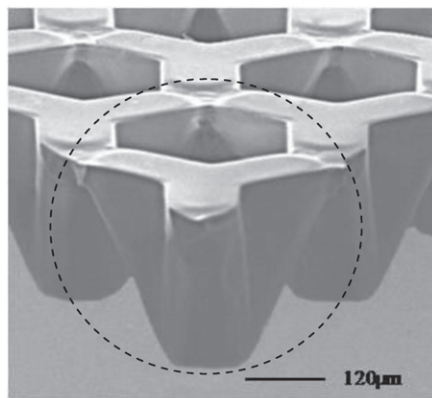
(b)

Figure 14. Micro horn arrays of 3D microstructures: (a) screwed wind vane array, (b) cardiac horn array.

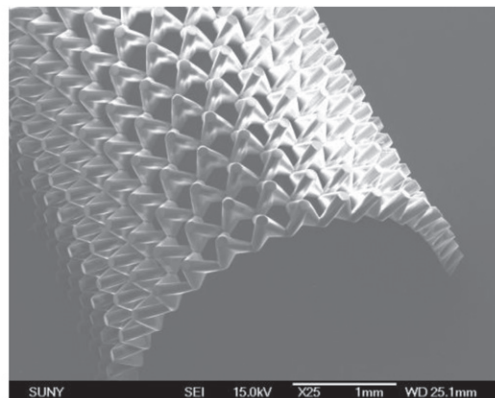
tracing simulation performed here provides a useful guideline for the overall 3D pattern design.

One of the advantages of UV lithography is that array structures can be produced using an array mask pattern. Figures 14(a) and (b) are the screwed wind vane array with double blades and the cardiac horn array, respectively, showing the mass production capability of the dynamic mode multidirectional UV lithography process. Figure 14 shows an array with each unit structure isolated, where the pitch between neighboring structures is larger than the dimension of the unit structure. Meanwhile, the unit structure can also be constructed in a connected fashion to form a large-scale mesh structure, where the pitch between the neighboring structures is smaller than the lateral dimension of the unit structure. Figure 15 shows a fabricated structure in a connected fashion, where a three-leaf triangular slab is used as a unit structure. The fabricated unit structures overlap each other to form a unique large-scale mesh or membrane structure, where it shows a hexagonal shape on the top and a tapered pillar array on the bottom. The photomask used for this structure has a transparent circular pattern array in a dark field where the diameter of each circle is $60\ \mu\text{m}$ and the pitch between pillars is $121\ \mu\text{m}$. After $270\ \mu\text{m}$ thick SU-8 photoresist is applied on the prepared photomask, UV exposure is performed with the tilting angle varying from 0° to 58° and a rotational angle offset of 0° , 120° and 240° for each vertical triangular blade formation. Post-exposure bake and development complete the process. Since this membrane has a continuous hexagonal mesh structure on the top providing a fixed end, and a tapered pillar array on the bottom resulting in an open end, the membrane is easily bent to form a curved structure. An initially flat membrane is soaked in acetone to soften it and results in a rounded membrane as shown in figure 15(b).

In multidirectional UV lithography, the control of the UV exposure dose is one of the key parameters. For a high aspect ratio 3D structure with backside exposure, the UV power is higher at the bottom and lower at the top because of energy absorption in the polymer layer as light propagates in the slab. Some structures patterned with insufficient optical dose are shown in figure 16 and in [39]. The SEM images are colored

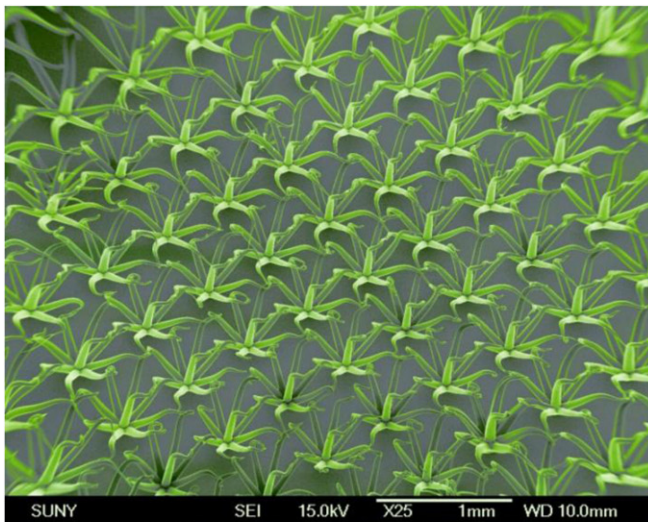


(a)

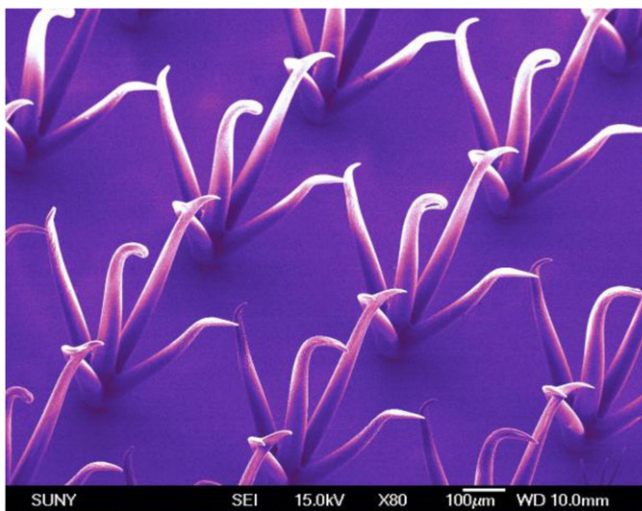


(b)

Figure 15. Fabrication of a large-scale membrane using dynamic mode multidirectional UV lithography with unit cells connected to each other: (a) unit cell consisting of three vertical triangular slabs, (b) rounded membrane upside down.



(a)



(b)



(c)

Figure 16. Deformed 3D microstructures due to insufficient optical dose and prolonged development revealing artistic features (SEM images are colored for aesthetic purpose): each one has a nickname: (a) ‘United We Stand’, (b) ‘Dancing Microswans’, (c) ‘Sea Anemone’.

by the authors for aesthetic purpose. Figures 16(a) and (b) show structures with multiple branches with a soft baking time of 5 h and an SU-8 layer thickness of $500\ \mu\text{m}$, an UV exposure dose of each branch of $2400\ \text{mJ cm}^{-2}$ for figure 16(a) and $1600\ \text{mJ cm}^{-2}$ for figure 16(b), a post-exposure baking time of 1 h at $95\ ^\circ\text{C}$ and a developing time of 30 min with slight stirring. When SU-8 is not completely cross-linked, it tends to be developed/dissolved out continuously when it is left in the development bath. Therefore, the top portion becomes thin after development. After development, when the sample is taken out of the liquid develop into the air for drying, surface tension at the interface between developer and air causes deformation of the tip. Figure 16(c) shows that the structure has relatively large tips and bottom. It is attributed to multiple factors including UV energy dose, scattering and diffraction of the UV light at the tip.

6. Conclusion

We have demonstrated automated dynamic mode multidirectional UV lithography and produced various complex structures from single and array mask patterns. Dynamic mode UV lithography has additional process parameters, such as initial and final tilting and rotational angles, their angular velocities, and synchronization between inclined and rotational motions, in addition to the parameters in the static mode multidirectional UV exposure such as tilting angle, refractive index of the photoresist and thickness of the photoresist. By combining and varying these parameters, a variety of complex 3D structures have been produced. To demonstrate the versatility of the process for 3D microfabrication, a vertical reverse triangular slab, a vertical reverse quadruple triangular slab, a cardiac horn, screwed wind vanes with two blades and four blades, a horn with the figure ‘8’ shape, a horn with the embedded figure ‘8’, a bowtie horn, a four-leaf clover horn and a horn with a flower shape (la flor) have been successfully fabricated. Ray tracing simulation has been performed using mathematical equations and a math tool (MathCAD). The overall shapes of the fabricated structures and the simulated ones agree very well. These kinds of 3D structures find great potential for radio frequency (RF)/microwave applications such as integrated millimeter wave and terahertz antennas and waveguides, 3D photonic bandgap (PBG) structures, 3D metamaterials, as well as microfluidic applications such as rotors and microturbines.

Acknowledgment

This work has been sponsored by the National Science Foundation (CAREER: ECCS 0748153 and CMMI 0826434).

References

- [1] Ehrfeld W, Gotz F, Munchmeyer D, Schelb W and Schmidt D 1988 LIGA process: sensor construction techniques via x-ray lithography *Proc. Solid-State Sensor and Actuator Workshop (Hilton Head Island, SC, 1988)* pp 1–4
- [2] Bley P, Gottert J, Harmening M, Himmelhaus M, Menz W, Mohr J, Muller C and Wallrabe U 1991 The LIGA process for the fabrication of micromechanical and microoptical

- components *Microsystem Technologies* (Berlin: Springer) pp 302–14
- [3] Behrmann G P and Duignan M T 1997 Excimer laser micromachining for rapid fabrication of diffractive optical elements *Appl. Opt.* **36** 4666–76
 - [4] Li Y and Sugiyama S 2004 X-ray lithography mask fabricated by excimer laser process *Proc. SPIE* **5641** 316
 - [5] Engelmann G, Ehrmann O, Simon J and Reichl H 1990 Development of a fine pitch bumping process *Microsystem Technologies 90* ed H Reichl (Berlin: Springer) pp 435–40
 - [6] Furukawa S, Miyajima H, Mehregany M and Liu C C 1993 Electroless plating of metals for micromechanical structures *Technical Digest, IEEE Solid-State Sensors and Actuators Workshop (Yokohama, Japan, June 1993)* pp 66–9
 - [7] Frazier A B and Allen M G 1992 High aspect ratio electroplated microstructures using a photosensitive polyimide process *Proc. MEMS '92 Travemunde (Germany)* pp 87–92
 - [8] Gobet J, Cardot F, Bergqvist J and Rudolf F 1993 Electrodeposition of 3D microstructures on silicon *J. Micromech. Microeng.* **3** 123–30
 - [9] Lorenz H, Despont M, Fahrni N, LaBianca N, Renaud P and Vettiger P 1997 SU-8: a low-cost negative resist for MEMS *J. Micromech. Microeng.* **7** 121–24
 - [10] Cros F and Allen M G 1998 High aspect ratio structures achieved by sacrificial conformal coating *Proc. Solid-State Sensor and Actuator Workshop (Hilton Head Island, SC, 1998)* pp 261–4
 - [11] Zhang J, Tan K L, Hong G D, Yang L J and Gong H Q 2001 Polymerization optimization of SU-8 photoresist and its applications in microfluidic systems and MEMS *J. Micromech. Microeng.* **11** 20–6
 - [12] Lee K Y, LaBianca N, Rishton S A, Zolgharnain S, Gelorme J D, Shaw J and Chang T H-P 1995 Micromachining applications of a high resolution ultrathick photoresist *J. Vac. Sci. Technol.* **13** 3012–6
 - [13] MicroChem. Inc. SU-8 data sheets (online). Available at http://www.microchem.com/products/su_eight.htm
 - [14] Yoon Y-K, Park J-W and Allen M G 2005 Polymer-core conductor approaches for RF MEMS *J. Microelectromech. Syst.* **14** 886–94
 - [15] Choi Y, Powers R, Yoon Y-K and Allen M G 2003 A three-dimensional microfluidic network for cellular perfusion *7th Int. Conf. on Miniaturized Chemical and Biochemical Analysis Systems (MicroTAS2003)* pp 1001–4
 - [16] Pan B, Yoon Y, Zhao Y Z, Papapolymerou J, Tentzeris M M and Allen M 2005 A broadband surface-micromachined 15–45 GHz microstrip coupler *IEEE MTT-S Int. Microwave Symp. Dig. (Long Beach, CA, June 2005)* pp 989–92
 - [17] Yoon Y-K, Pan B, Papapolymerou J, Tentzeris M M and Allen M G 2005 Surface-micromachined millimeter-wave antennas *Proc. 13th Int. Solid-State Sensors, Actuators and Microsystems Conf. (Transducers 2005)* vol 2 pp 1986–89
 - [18] Pan B, Yoon Y-K, Ponchak G E, Allen M G, Papapolymerou J and Tentzeris M M 2006 Analysis and characterization of a high performance Ka-band surface micromachined elevated patch antenna *IEEE Antennas Wireless Propag. Lett.* **5** 511–4
 - [19] Yoon Y-K, Pan B, Papapolymerou J, Tentzeris M M and Allen M G 2005 A vertical W-band surface-micromachined Yagi-Uda antenna *IEEE AP-S Int. Symp. (Washington, DC)* pp 594–7
 - [20] Pan B et al 2004 A W-band surface micromachined monopole for low-cost wireless communication systems *Proc. IEEE Int. Microwave Symp. (Fort Worth, TX, June 2004)* pp 1935–8
 - [21] Beuret C, Racine G A, Gobet J, Luthier R and de Rooij N F Microfabrication of 3D multidirectional inclined structures by UV lithography and electroplating *Proc. IEEE Int. Conf. on MEMS (MEMS '94)* pp 81–5
 - [22] Sato H, Kakinuma T, Go J S and Shoji S 2004 In-channel 3D micromesh structures using maskless multi-angle exposures and their microfilter application *Sensors Actuators A* **111** 87–92
 - [23] Sato H, Yagyu D, Ito S and Shoji S 2006 Improved inclined multi-lithography using water as exposure medium and its 3D mixing microchannel application *Sensors Actuators A* **128** 183–90
 - [24] Yoon Y-K, Park J-H, Cros F and Allen M G 2003 Integrated vertical screen microfilter system using inclined SU-8 structures *Proc. IEEE Microelectromechanical Systems Conf. (MEMS) (Kyoto Japan)* pp 227–30
 - [25] Sato H, Yagyu D, Ito S and Shoji S 2006 Improved inclined multi-lithography using water as exposure medium and its 3D mixing microchannel application *Sensors Actuators A* **128** 183–90
 - [26] Han M, Hyun D-H, Park H-H, Lee S S, Kim C-H and Kim C G 2007 A novel fabrication process for out-of-plane microneedle sheets of biocompatible polymer *J. Micromech. Microeng.* **17** 1184–91
 - [27] Tseng F-G and Hu H-T 2003 A novel micro optical system employing inclined polymer mirrors and Fresnel lens for monolithic integration of optical disk pickup heads *12th Int. Conf. on Transducers, Solid-State Sensors, Actuators and Microsystems* vol 1 pp 599–602
 - [28] Han M, Lee W, Lee S-K and Lee S S 2003 Fabrication of 3D microstructures with inclined/rotated UV lithography *Proc. IEEE Micro Electro Mechanical Systems* pp 554–7
 - [29] Han M, Lee W, Lee S-K and Lee S S 2004 3D microfabrication with inclined/rotated UV lithography *Sensors Actuators A* **111** 14–20
 - [30] Yoon Y-K, Park J-H and Allen M G 2006 Multidirectional UV lithography for complex 3D MEMS Structures *IEEE J. MEMS* **15** 1121–30
 - [31] Wang P-C, Wester B A, Rajaraman S, Paik S-J, Kim S-H and Allen M G 2009 Hollow polymer microneedle array fabricated by photolithography process combined with micromolding technique *31st Annual Int. Conf. IEEE EMBS (Minneapolis, MN USA, 2–6 September 2009)* pp 7026–9
 - [32] Park J-H, Allen M G and Prausnitz M R 2005 Biodegradable polymer microneedles: fabrication, mechanics and transdermal drug delivery *J. Control. Release* **104** 51–66
 - [33] Park J H, Yoon Y K, Choi S O, Prausnitz M R and Allen M G 2007 Tapered conical polymer microneedles fabricated using an integrated lens technique for transdermal drug delivery *IEEE Trans. Biomed. Eng.* **54** 903–13
 - [34] Yoon Y-K and Allen M G Proximity mode inclined UV lithography *Solid-State Sensor, Actuator, and Microsystems Workshop (Hilton Head Island, SC, 4–8 June 2006)* pp 98–99
 - [35] Kim J, Allen M G and Yoon Y-K 2008 Automated dynamic mode multidirectional UV lithography for complex 3D microstructures *IEEE 21st Int. Conf. on Micro Electro Mechanical Systems (13–17 January 2008)* pp 399–402
 - [36] Yang R and Wang W 2005 A numerical and experimental study on gap compensation and wavelength selection in UV-lithography of ultra-high aspect ratio SU-8 microstructures *Sensors Actuators B* **110** 279–88
 - [37] Zhu Z, Zhou Z-F, Huang Q-A and Li W-H 2008 Modeling, simulation and experimental verification of inclined UV lithography for SU-8 negative thick photoresists *J. Micromech. Microeng.* **18** 125017
 - [38] Zhou Z, Huang Q-A, Li W, Lu W, Zhu Z and Feng M 2007 The swelling effects during the development processes of deep UV lithography of SU-8 photoresists: theoretical study, simulation and verification *IEEE Sensors. J.* **325**–8
 - [39] Kim J and Yoon Y-K 2010 Microworld: united we stand *Lab Chip* **10** 669